10-26-2015

Geomagnetic paleointensity in historical pyroclastic density currents: Testing the effects of emplacement temperature and postemplacement alteration

Julie A. Bowles
University of Wisconsin-Milwaukee, bowlesj@uwm.edu

Jeffrey S. Gee
University of California - San Diego, jsgee@ucsd.edu

Mike J. Jackson
University of Minnesota - Twin Cities, jacks057@umn.edu

Margaret S. Avery
University of Minnesota - Twin Cities

AGU PUBLICATIONS

Geochemistry, Geophysics, Geosystems

RESEARCH ARTICLE
10.1002/2015GC005910

Key Points:
- Small pyroclastic flows are suitable for paleointensity studies
- Emplacement temperature indirectly affects paleointensity by controlling magnetic mineralogy
- Sample water content is linked to paleointensity and may be used as indicator of alteration

Supporting Information:
- Supporting Information S1
- Table S2
- Table S3

Correspondence to:
J. A. Bowles,
bowlesj@uwm.edu

Citation:
Bowles, J. A., J. S. Gee, M. J. Jackson, and M. S. Avery (2015), Geomagnetic paleointensity in historical pyroclastic density currents: Testing the effects of emplacement temperature and postemplacement alteration, *Geochem. Geophys. Geosyst.*, *16*, 3607–3625, doi:10.1002/2015GC005910.

Received 11 MAY 2015
Accepted 25 SEP 2015
Accepted article online 1 OCT 2015
Published online 26 OCT 2015

Geomagnetic paleointensity in historical pyroclastic density currents: Testing the effects of emplacement temperature and postemplacement alteration

Julie A. Bowles[1], Jeffrey S. Gee[2], Mike J. Jackson[3], and Margaret S. Avery[2]

[1]Department of Geosciences, University of Wisconsin – Milwaukee, Milwaukee, Wisconsin, USA, [2]Scripps Institution of Oceanography, University of California, San Diego, California, USA, [3]Institute for Rock Magnetism, Winchell School of Earth Sciences, University of Minnesota, Minneapolis, Minnesota, USA

Abstract Thellier-type paleointensity experiments were conducted on welded ash matrix or pumice from the 1912 Novarupta (NV) and 1980 Mt. St. Helens (MSH) pyroclastic density currents (PDCs) with the intention of evaluating their suitability for geomagnetic paleointensity studies. PDCs are common worldwide, but can have complicated thermal and alteration histories. We attempt to address the role that emplacement temperature and postemplacement hydrothermal alteration may play in nonideal paleointensity behavior of PDCs. Results demonstrate two types of nonideal behavior: unstable remanence in multidomain (MD) titanomagnetite, and nonideal behavior linked to fumarolic and vapor phase alteration. Emplacement temperature indirectly influences MSH results by controlling the fraction of homogenous MD versus oxyexsolved pseudo-single domain titanomagnetite. NV samples are more directly influenced by vapor phase alteration. The majority of NV samples show distinct two-slope behavior in the natural remanent magnetization—partial thermal remanent magnetization plots. We interpret this to arise from a (thermo)chemical remanent magnetization associated with vapor phase alteration, and samples with high water content (>0.75% loss on ignition) generate paleointensities that deviate most strongly from the true value. We find that PDCs can be productively used for paleointensity, but that—as with all paleointensity studies—care should be taken in identifying potential postemplacement alteration below the Curie temperature, and that large, welded flows may be more alteration-prone. One advantage in using PDCs is that they typically have greater areal (spatial) exposure than a basalt flow, allowing for more extensive sampling and better assessment of errors and uncertainty.

1. Introduction

One of the challenges in determining past variations in the absolute intensity of the geomagnetic field lies in finding materials that have ideal, single-domain (SD) particles that are also resistant to alteration on heating. True SD particles are rare in nature. Lava flows, which cool relatively quickly, are frequently used in paleointensity studies because they typically contain pseudo-single-domain (PSD) sized particles, often viewed as a reasonable compromise. Many paleointensity studies have been carried out on basaltic lava flows [e.g., *Coe*, 1967b; *Kono*, 1974; *Dunlop and Hale*, 1976; *Coe et al.*, 1978; *Senanayake et al.*, 1982; *Roperch et al.*, 1988; *Prévot et al.*, 1990; *Goguitchaichvili et al.*, 2004; *Yamamoto et al.*, 2003; *Biggin et al.*, 2009; *Camps et al.*, 2011; *Kulakov et al.*, 2013], with variable success. In addition to nonideal grain size, some flows are particularly prone to alteration during paleointensity experiments, often either by oxidation and/or inversion of (titano-)maghemite to magnetite or hematite [e.g., *Özdemir*, 1987; *Draeger et al.*, 2006; *Herrero-Bervera and Valet*, 2009]. Restricting paleointensity studies to basalts also restricts us in space and time to localities with basaltic volcanism. It would therefore be advantageous if paleointensity estimates could be derived from a wider variety of eruptive units, including more silicic units, which tend to erupt explosively often forming ash and/or pumice-rich pyroclastic density currents (PDCs).

PDCs (many with high quality $^{40}Ar/^{39}Ar$ ages) are common worldwide and particularly in the southwestern U.S. Thus, if absolute paleointensities can be determined from ash flows, it may be possible to compile a more comprehensive database of past field intensity fluctuations. It has been demonstrated that fine-grained SP-SD magnetite can exist in the glassy matrix or vitrophyre glass of ash flow tuffs [*Geissman et al.*, 1983;

Schlinger et al., 1988a, 1988b, 1991; *Till et al*., 2011], and the glass may at least partially shield the magnetite from alteration after emplacement and during laboratory heating. These potential advantages make them attractive targets for paleointensity studies, but PDCs can have complicated thermal and alteration histories, leaving the nature of magnetic remanence in these flows uncertain.

The postemplacement history of PDCs controls two important aspects of remanence acquisition. First, the primary magnetic mineralogy of tuffs may be significantly changed during postemplacement cooling and alteration, particularly associated with vapor phase alteration. For example, many ash flows contain phenocrysts of (titano)magnetite that may be oxidized to (titano)maghemite or hematite [e.g., *Rosenbaum*, 1993; *Schlinger et al*., 1991] or that may experience oxyexsolution [*Reynolds*, 1977]. In addition, secondary, fine-grained (SP-SD) magnetite may be produced during slow cooling [*Geissman et al*., 1983; *Schlinger et al*., 1988a, 1988b, 1991; *Till et al*., 2011], particularly in welded flows. Second, the cooling history determines whether magnetic particles will acquire a total thermoremanent magnetization (TRM), a partial thermoremanence (pTRM), a chemical remanence (CRM), or some combination of thermochemical remanence (TCRM).

Compared to basaltic flows, paleointensity has not been extensively tested in pyroclastic flows, and results have been mixed. The first reported paleointensity attempt on welded ash flow tuffs [*Reynolds*, 1977] involved Thellier-type experiments on six specimens representing three different welded tuffs (0.64–2.08 Ma) [*Lanphere et al*., 2002; *Rivera et al*., 2014; *Singer et al*., 2014] of the Yellowstone Group in the American West. *Tanaka et al*. [1994] and *Takai et al*. [2002] conducted Thellier-type paleointensity experiments on 14–45 ka pyroclastic flows on Hokkaido, Japan, although it is not specified what type of material was sampled from the flows. Roughly, one half to two thirds of the sites were interpreted as successful, although many of the NRM-pTRM (Arai) plots showed two-slope behavior, and the authors interpreted only the high-temperature slope. *Schnepp* [1995] studied ~400 ka nonwelded, zeolitized tuffs from the East Eifel volcanic field (Germany), deposited at ~500°C. Most samples strongly altered at $T > 300$°C, and in this instance interpretation was limited to the low-temperature fraction. Although results were internally consistent, the author considered the results to be unreliable because the samples were strongly viscous. Thellier-type [*Takai et al*., 2002] and Shaw-type [*Mochizuki et al*., 2013] tests were conducted on 90–270 ka welded tuffs and pyroclastic flow deposits from Kyushu, Japan, and the two methods were in general agreement. Shaw-type experiments on 5–500 ka pyroclastic deposits from Unzen volcano, Japan, [*Yamamoto et al*., 2010] yielded six sites with internally consistent results and another four with more variable results. *Perrin et al*. [2013] worked with 20.4–31.0 Ma rhyolitic ignimbrites, and in this case Thellier-type paleointensity experiments produced results of high technical quality, but with no internal consistency. Combined with the presence of maghemite and hematite, the authors concluded that these results were unreliable and that hydrothermal alteration had affected the magnetization. *Roperch et al*. [2014] sampled several locations where juvenile scoria was incorporated in PDCs. They found that the SD to PSD-sized grains found in the scoria typically resulted in Thellier-type paleointensity estimates of high technical quality. One historical flow was sampled, and the anisotropy and cooling-rate corrected result was in approximate agreement with the expected field. Finally, *Paterson et al*. [2010b] conducted Thellier-type experiments on lithic clasts incorporated into flows from Mt. St. Helens (erupted 1980), Lascar (erupted 1993), and Vesuvius (erupted 472 A.D.). They determined that the lithic clasts have promise for paleointensity studies, but can still suffer from problems common to lava flows, including multidomain effects.

In all of the studies, the number of specimens analyzed per cooling unit is relatively low in terms of assessing overall flow-wide variability. With the exception of *Takai et al*. [2002] and *Paterson et al*. [2010b] where up to 27 "successful" specimens (as defined by the authors) per cooling unit are identified, 10 or fewer "successful" results are reported for each cooling unit. Given the potential spatial variability in cooling and hydrothermal activity, a large-scale evaluation of how magnetic mineralogy, cooling history, emplacement temperature, and alteration may control paleointensity is in order.

By contrast, preliminary work from the ~0.76 Myr Bishop Tuff [*Gee et al*., 2010] sampled at multiple locations in the cooling unit, as well as in variably welded and variably altered zones. Thellier-type paleointensity experiments were conducted on 89 specimens. Forty-six were interpreted, and the results were internally consistent with moderately high technical quality. Although promising, the authors noted that the samples carried both magnetite and (titano)maghemite and that a significant fraction of the remanence unblocked at $T > 580$°C. The high-temperature ($T > 580$°C) data typically resulted in a higher paleointensity, and this

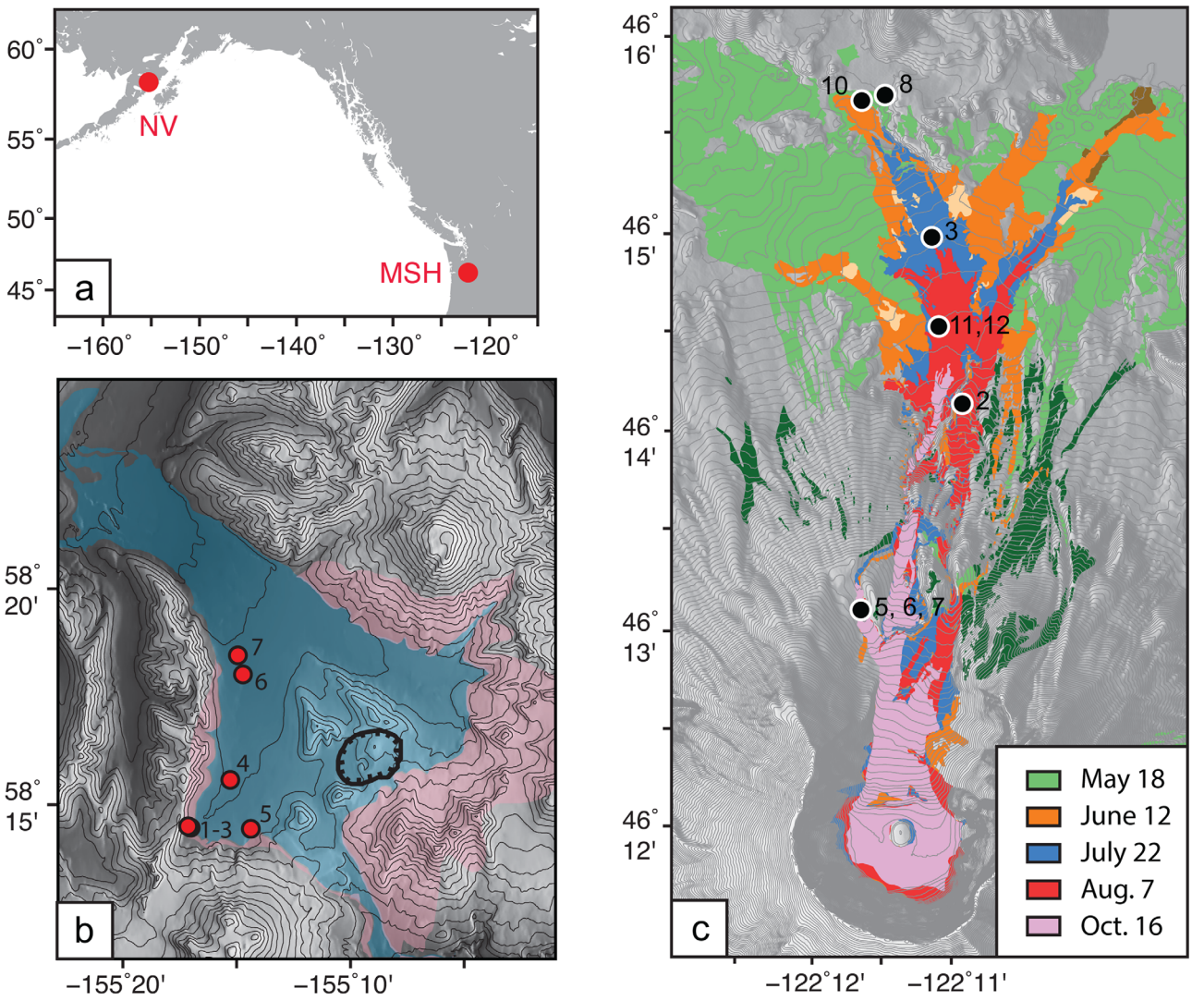

Figure 1. Maps of study areas. (a) Overview map showing locations of Novarupta (NV) and Mt. St. Helens MSH. (b) Novarupta sampling locations. Pink shaded area denotes extent of the all rhyolite ignimbrite that formed the first phase of the eruption. Blue shaded area represents successive phases with increasing amounts of andesite and dacite. Sampling locations are all in the more andesitic and dacitic flows. Flow boundaries and vent location (heavy black line) from *Fierstein and Wilson* [2005]. (c) Mt. St. Helens sampling locations. Pyroclastic flow units of the 1980 eruptive sequence [*Kuntz et al.*, 1990] denoted by colored shading.

component was interpreted as a CRM held by the maghemite and derived from high-temperature vapor-phase alteration. Thus, only the low-temperature slopes were used in interpretation. More recent work on the Bishop tuff has resulted in less internally consistent results, demonstrating the impact non-TRM remanence may have on paleointensity estimates if misinterpreted as TRM [*Avery et al.*, 2012].

Because of the mixed results derived from older PDCs, we undertook this study on two historical pyroclastic flows where field strength is known. This allows us to test potential nonideal behavior arising from variations in emplacement temperature or degree of postemplacement hydrothermal alteration, as well as magnetic mineralogy. In this study we explicitly avoid lithic fragments, focusing instead on the relatively glassy pumice or welded ash matrix, in order to specifically test the fidelity of these glassy materials. To our knowledge, these are the only reported paleointensity results on historical PDCs not derived from lithic fragments.

1.1. Geologic Settings

1.1.1. Novarupta Eruption, 1912, Valley of Ten Thousand Smokes

The 1912 Novarupta (NV) eruption in southern Alaska (Figure 1b) deposited approximately 11 km^3 of ash flows over a 60 h period [*Fierstein and Wilson*, 2005; *Hildreth*, 1987; *Hildreth and Fierstein*, 2000]. The flows

were confined to a valley that narrows northward away from the vent, and due to extensive fumarolic activity the valley now bears the name Valley of Ten Thousand Smokes (VTTS). The initial flows were rhyolitic with subsequent eruptions having increasing proportions of andesitic and dacitic material [*Fierstein and Wilson*, 2005]. Titanomagnetite is present as phenocrysts in pumice of all compositions and as inclusions in pyroxene in the intermediate rocks [*Hildreth*, 1983]. The valley-filling outflow sheets are nonwelded in the lower valley but increasingly indurated nearer the vent, where flow thickness is >170 m [*Kienle*, 1991]. Fumarole temperatures as high as 645°C were measured at ~3 km from the vent in 1919 [*Zies*, 1924], providing a minimum emplacement temperature for near-vent deposits. Although the temperature of most fumaroles had decreased to ~30°C by the 1980s, discovery of a moderate temperature vent in 1987 provides evidence for a still hot (~200°C) zone at depth [*Hogeweg et al*., 2005].

Based on oxygen isotope data of both feldspar phenocrysts and groundmass, the VTTS tuff has experienced a two-stage fumarolic history [*Holt and Taylor*, 2001]: relatively focused short-lived (10–15 years), high-temperature (>450°C) vigorous fumarolic activity followed by more widespread long term (possibly continuing to present day) low-temperature (<150°C) vapor phase venting. The effects of the high-temperature stage are localized, and $^{18}O/^{16}O$ evidence for interaction with high-temperature meteoric water is found up to only a few centimeters to a few meters from fumarolic fissures [*Holt and Taylor*, 2001]. There is typically a strong zonation from leached white, to pink and unaltered grey tuff away from the conduit over the scale of centimeters to meters. Chemical alteration associated with the high-temperature phase includes a leaching of iron that persists up to several tens of centimeters away from the fissure [*Papike et al*., 1991].

1.1.2. Mt. St. Helens Eruptions, 1980

The 1980 eruptions of Mt. St. Helens began on 18 May with an earthquake-triggered collapse of the inflated north flank of the volcano [*Christiansen and Peterson*, 1981; *Rosenbaum and Waitt*, 1981]. The rapid unloading triggered a series of northward-directed hydrothermal steam blasts, followed by a dacitic eruption which produced a Plinian ash column and deposited voluminous pumiceous ash flows on the north slope. Subsequent eruptions on 25 May, 12 June, 22 July, 7 August, and 17 October were smaller in scale but each left significant deposits of nonwelded dacitic pumice and ash [*Christiansen and Peterson*, 1981].

On eruption, the turbulent pyroclastic flows cooled in transit by entrainment of air and of previously deposited material eroded by the flows, especially on the higher portions of the north flank of the volcano. Farther downslope on the "pumice plain," deposition dominated over erosion, and flow units are typically a few meters in thickness [*Rowley et al*., 1981]. Emplacement temperatures were estimated by temperature-depth profiles measured days to months after most eruptions [*Banks and Hoblitt*, 1996]. In general, emplacement temperatures were lowest for the 18 May pyroclastic flow (300–420°C), increasing for the later events to up to ~850°C on 17 October. Emplacement temperatures generally were highest near the eruptive source, decreasing by about 200°C over the first few hundred meters, and thereafter much more slowly with distance [*Banks and Hoblitt*, 1996].

2. Methods

2.1. Field Sampling

One-inch diameter oriented cores were sampled at both localities with a battery-powered drill. The Novarupta samples (Figure 1b) were all taken from the upper, more andesite-rich and dacite-rich flows, the upper 30–40 m of which are exposed in steep-sided gorges along the River Lethe and Knife Creek. Samples were dominantly poorly to moderately welded ash flow, frequently with small (mm to cm-sized) pumice and lithic fragments distributed in the ash matrix. At one site (Site 4), samples were collected horizontally across two fossil fumarole fissures that showed visible leaching up to ~6 cm on either side of the fissure (discussed below). At Mt. St. Helens (Figure 1c), cores were drilled from large (10–50 cm diameter) pumice blocks contained in the ash matrix. In a few cases where the blocks were too small to core, they were taken as oriented block samples. At site 2, lithic fragments 10–20 cm in diameter were also sampled, and thermal demagnetization of these samples was used to estimate emplacement temperature [e.g., *Hoblitt and Kellogg*, 1979; *Paterson et al*., 2010a]. At both localities, efforts were made to sample as widely as possible throughout the flows, both in areal extent (Figure 1) and depth in flow. At NV, samples were typically collected vertically over ~1.5–5 m of section at each site, while the thinner flows at MSH were typically sampled over < 1.5 m. Site locations are given in supporting information Table S1.

2.2. Magnetic Experiments

Bulk room-temperature susceptibility was measured on a Magnon Variable Frequency Susceptibility Meter. Temperature dependent susceptibility χ(T) (up to 600°C or 700°C) was measured on a Kappabridge KLY-2 with CS-2 furnace or MFK1-FA with CS-4 furnace, under air (MSH) or flowing Ar (NV) atmosphere. All measurements were made at the Institute for Rock Magnetism (IRM) at the University of Minnesota with the exception of the χ(T) measurements made on the MFK1 which were conducted at the University of Wisconsin – Milwaukee (UWM). Curie temperatures were estimated by finding the (negative) peak in the first derivative of the χ(T) data.

Magnetic hysteresis was measured at the IRM on a Princeton Measurements Corporation vibrating sample magnetometer in fields up to 1 T, and hysteresis data were processed as in *Jackson and Solheid* [2010]. To discriminate hysteresis properties of magmatic phenocrysts from possible glass-hosted magnetite, heavy liquids were used to separate several specimens from each locality (NV and MSH) into low-density and high-density fractions. Heavy liquids of 2450 kg m^{-3} (NV) or 2420 kg m^{-3} (MSH) were used in the separation process described in *Lagroix et al*. [2004].

A subset of specimens from each locality was subjected to further analysis in the form of the Lowrie three-axis isothermal remanent magnetization (IRM) experiment [*Lowrie*, 1990]. A saturation IRM was acquired in steps, with a maximum applied field of 2.5 T. This saturation IRM was overprinted by IRMs in fields of 0.4 and 0.1 T, applied in orthogonal directions in order to separate the high-coercivity, intermediate-coercivity, and low-coercivity spectra. The samples were then thermally demagnetized in air to provide information on the blocking temperature spectra of the various coercivity fractions. These experiments were performed at the Scripps (SIO) Paleomagnetic Lab.

Stepwise thermal demagnetization (up to 600°C or 610°C) of the NRM in air was carried out on a subset of oriented specimens from each locality. Alternating field (AF) demagnetization was carried out on a subset of oriented specimens from Novarupta only. MSH thermal demagnetization and AF demagnetization of NV samples were conducted at the IRM, while thermal demagnetization of NV samples was conducted at SIO.

Thellier-type paleointensity experiments [*Thellier and Thellier*, 1959] were conducted in air at SIO on unoriented specimens in 25°C steps between 100°C and 600°C or 650°C, using a laboratory field of 54 μT or 40 μT. We used the IZZI (In field – Zero field, Zero field – In field) protocol [*Tauxe and Staudigel*, 2004; *Yu et al*., 2004], which alternates the order in which the in-field and zero-field treatments are applied in order to highlight behavior arising from nonreciprocity of partial thermal remanent magnetization (pTRM). pTRM checks [*Coe*, 1967a] were carried out on alternate temperature steps.

Finally, selected specimens from Novarupta were subjected to viscosity experiments modeled after *Prévot* [1981]. See supporting information text for additional information.

2.3. Loss on Ignition (LOI)

Loss on ignition was performed on a subset of NV specimens to test the effects of sample hydration on paleointensity. Samples were powdered, dried overnight at 120°C, and then heated at 1050°C for 15 min. Mass loss during the 1050°C heating is assumed to be water.

3. Results

3.1. Magnetic Mineralogy

For both localities, the χ(T) data are mostly reversible, meaning that starting and ending room-temperature susceptibilities are nearly the same (Figure 2). Notable exceptions are found in NV specimens taken from visibly altered fumarolic zones (e.g., Figures 2c and 2d). Curie temperatures (T_c) are consistent with a Ti-rich titanomagnetite (T_c ranging between approximately 350°C and 500°C) and a Ti-poor magnetite ($T_c > 525$°C). Reflected light microscopy and electron microprobe data [*Bowles et al*., 2013; *Jackson and Bowles*, 2014] show that the Ti-rich phase is optically homogeneous, with moderate amounts of Mg-substitution and Al-substitution, while the Ti-poor phase has ilmenite lamellae characteristic of high-temperature oxidation exsolution. Both phases are present as phenocrysts up to ~200 μm diameter.

The homogenous titanomagnetite grains frequently have Curie temperatures that are higher measured on warming compared to those measured on cooling. This discrepancy has been interpreted as arising from

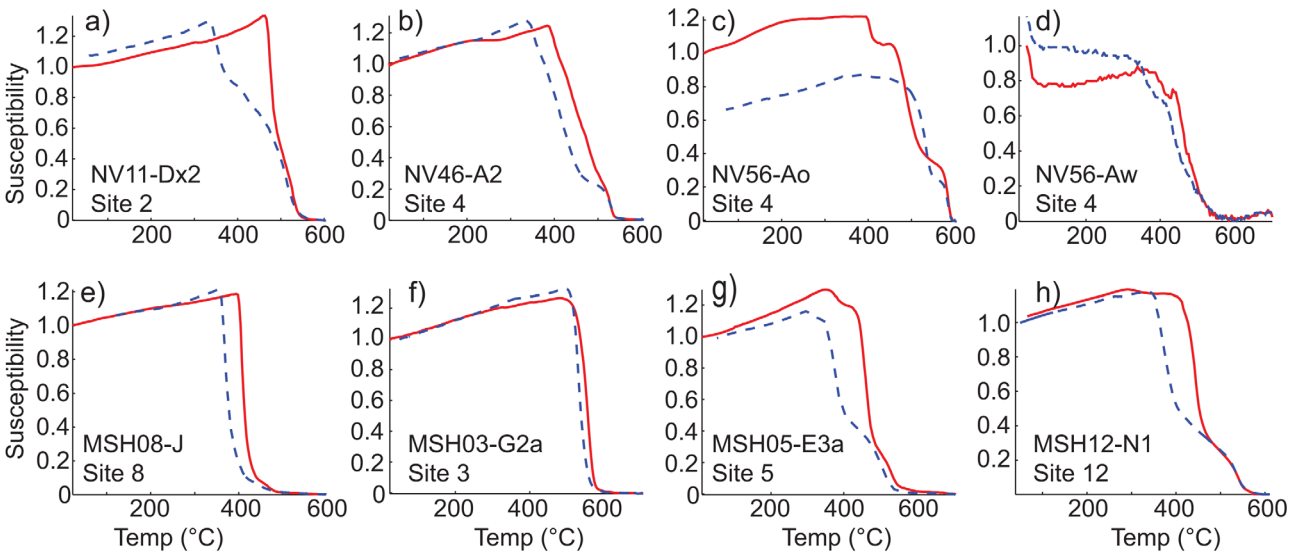

Figure 2. Thermomagnetic data from representative specimens. Solid red line measured on warming. Dashed blue line measured on cooling.

cation reordering in the crystal structure, as opposed to chemical alteration [*Bowles et al*., 2013; *Jackson and Bowles*, 2014], and means that the Curie temperature of many of our samples is strongly dependent on thermal history. The inferred cation reordering process is time-dependent and temperature-dependent, and the temperature at which reordering begins to take place on laboratory time scales is approximately 300°C. This phenomenon will play an important role in our discussion of the paleointensity results below.

Most NV samples have at least two Curie temperatures, representing homogenous and exsolved titanomagnetite in variable proportions. Three (Figure 2c) or four Curie temperatures are not uncommon, and in some cases samples have a broad zone of continuous magnetization loss suggesting considerable compositional variations (Figure 2b). In most cases all but the highest T_c exhibit the irreversible behavior described above that we attribute to cation reordering in the titanomagnetite. Two measured specimens showed evidence for a phase that orders at $T < 75$°C (e.g., Figure 2d), consistent with high-Ti titanomagnetite or titanohematite or possibly goethite. Both of these specimens were within visibly altered zones of focused hydrothermal activity. Most MSH samples also have both a low-Ti and a high-Ti phase, in variable proportions (Figures 2e–2h). Samples from Sites 2 and 8 are dominated by the high-Ti (low T_c) phase (Figure 2e), while Site 3 is dominated by the low-Ti (high-T_c) phase (Figure 2f). Samples from sites 7, 11, and 12 are variable in their thermomagnetic behavior, with many samples having three or more Curie temperatures.

Thermal demagnetization of 3-axis IRM (supporting information Figure S1) in NV samples shows that most are fully demagnetized by 580°C, with the exception of two specimens with a maximum unblocking temperature of ~620°C in the low-coercivity fraction (supporting information Figure S1c), which may be due to maghemite. The low-coercivity ($\leq$ 0.4 T) component dominates in all samples except two from fumarolic fissures which have a slightly greater contribution from the high-coercivity component (supporting information Figure S1a). MSH specimens are almost all dominated by a low-coercivity component that unblocks between 400°C and 600°C.

Hysteresis results from both localities are consistent with pseudo-single-domain (PSD) sized particles. (Figure 3; see supporting information Figure S2, e.g., loops.) The exceptions are MSH Sites 2, 5, and 8 which are dominated by the homogeneous (nonexsolved) titanomagnetites and are closer to a multidomain (MD) endmember (Figure 3a). The PSD grain size of these relatively small pyroclastic flows is in contrast to the single-domain (SD) to superparamagnetic (SP) grain size found in the larger, more densely welded rhyolitic Bishop Tuff [*Gee et al*., 2010] and Tiva Canyon Tuff [*Till et al*., 2011] (Figure 3c).

Although the magnetic properties of the bulk NV and MSH samples are dominated by the relatively coarse phenocryst oxides, the low-density (glass-rich) NV separate is characterized by a smaller magnetic grain size

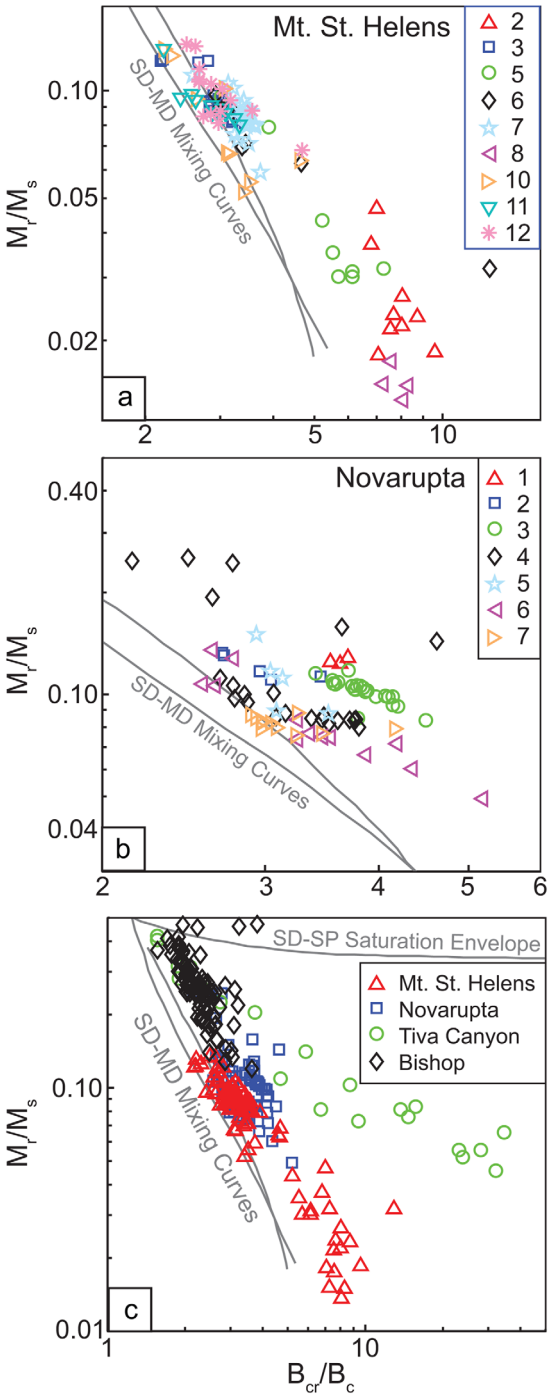

Figure 3. Hysteresis parameters by site for (a) Mt. St. Helens and (b) Novarupta. (c) Comparison with two larger flows. Tiva Canyon data from *Till et al.* [2011]. Bishop Tuff data from *Gee et al.* [2010]. Magnetite mixing curves from *Dunlop* [2002] are shown for reference only. Mr: saturation remanent magnetization; Ms: saturation magnetization; Bcr: coercivity of remanence; Bc: coercivity.

(supporting information Figure S3), possibly due either to magnetite precipitation out of the glass matrix, or to inclusions of magnetite in low-density silicate minerals. The same effect is not seen in the MSH density separates.

Bulk magnetic properties in the NV samples vary dramatically across fumarolic fissures (Figure 4). Susceptibility and saturation remanence (M_{rs}) decrease by over an order of magnitude, consistent with leaching of Fe from these zones [*Papike et al.*, 1991]. Coercivity and remanence ratio (M_{rs}/M_s) both increase, but not in a way consistent with a simple shift to finer-grain size. On the Day plot (Figure 3b), these altered Site 4 samples shift away from the SD-MD mixing curve (to the right), rather than along it. This may be due to mineralogical variation—for example, an increasing fraction of titanohematite or goethite—or to an increasing contribution from SP grains. The σ_{hys} shape parameter of *Fabian* [2003] increases for these samples, indicating a more wasp-waisted shape consistent with either mixing of high-coercivity and low-coercivity phases, or of PSD/SD and SP grain sizes. The 3-axis IRM results (above) suggest that it may be the former.

3.2. NRM Directions

Almost all samples show a single component of magnetization in both thermal and AF demagnetization. All specimens have principal component directions with a maximum angular deviation [*Kirschvink*, 1980] and a deviation angle [*Tauxe and Staudigel*, 2004] of $<10°$. Specimen-level results and locality means are shown in Figure 5. Site and locality means are detailed in supporting information Table S1. The MSH mean is indistinguishable from the expected 1980 Definitive Geomagnetic Reference Field (DGRF) direction, while the NV value is slightly shallower than the 1912 DGRF direction. This latter deviation is largely controlled by site 5, which may have undergone some post-emplacement rotation. If removed, the NV mean comes into statistical agreement with DGRF.

3.3. Paleointensity

Paleointensity results from Novarupta are mostly poorly behaved. Typical behavior includes a large loss of NRM (up to 50%) at low temperatures ($<$350–400°C) with very little pTRM gain (Figures 6c and 6d). The resulting paleointensity derived from the low-temperature slope is far higher (up to 200–400% greater) than the value of 55.2 μT expected from the DGRF, and that derived from the high-temperature slope is far lower (often $<$ 50%). A small number of samples have nearly linear Arai plots over the entire temperature interval and these slopes give paleointensity values approximately consistent with the expected value (Figures 6a

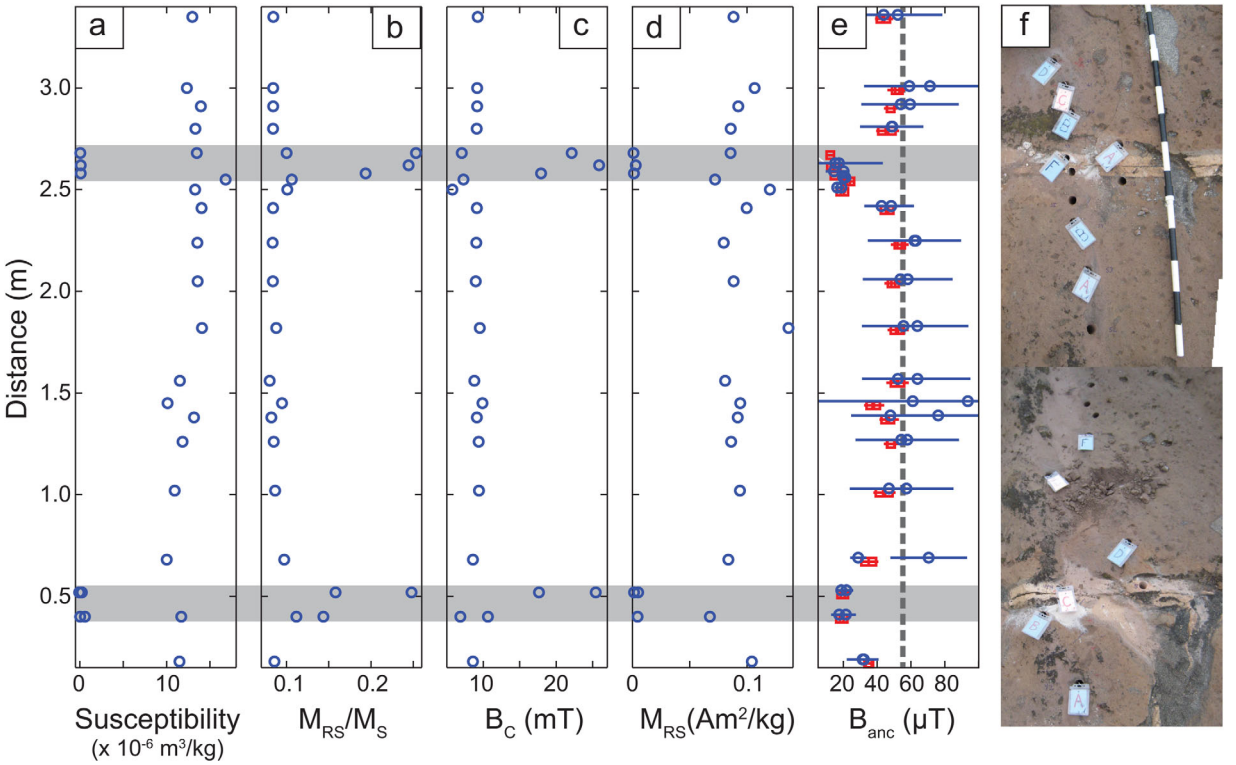

Figure 4. Section across two fumarolic cracks in the Novarupta deposit (Site 4). Distinct and spatially limited visible bleaching extends a few cm into the tuff. This is accompanied by a dramatic decrease in susceptibility and saturation remanence, and an increase in M_{RS}/M_S and B_c. Magnetic properties abruptly return to background values outside the bleached zones, but anomalous paleointensities persist for 10–20 cm beyond the zones. In Figure 4e, blue circles are paleointensity derived from bootstrap resampling and red squares are single-slope analyses (see text). Dashed gray line is DGRF field intensity.

and 6b). As a check on alteration during laboratory heating, we use the difference ratio (DRAT), defined as the difference between repeat pTRM steps, normalized by the length of the selected the NRM-pTRM segment, expressed as a percentage [*Selkin and Tauxe*, 2000]. For most specimens, the maximum DRAT is typically low ($<$10), for both low-temperature and high-temperature slopes, and would be interpreted as "passing" the pTRM check. There are no obvious rock magnetic properties (hysteresis, T_c, etc.) that distinguish the single-slope specimens from dual-slope specimens.

The MSH samples typically produce results of higher technical quality, and three types of behavior can be directly linked to magnetic mineralogy. Samples that are dominated by coarse-grained homogeneous titanomagnetite with Curie temperatures between ~350 and 500°C have univectoral decay up to ~350°C, accompanied by a highly scattered but linear Arai plot (Figure 7a). At $T > 350$°C, the directions become highly unstable, and any semblance of linearity in the Arai plot is lost. The break between relatively stable and relatively unstable behavior occurs at the temperature where cation reordering in these titanomagnetites becomes important on laboratory time scales, and T_c is evolving during the course of the experiment. The other endmember behavior is in samples dominated by oxyexsolved titanomagnetite with high T_c (Figure 7b). In this case, most of the NRM is unblocked at $T > 450$°C, and the resulting Arai plot is linear with passing pTRM checks. Samples with both magnetic phases show intermediate behavior (Figures 7c and 7d) where at $T < 300$–350°C pTRM checks show low DRAT values; from 350°C to 450°C or 500°C, the Arai plot departs from linearity and pTRM checks show higher DRAT values; and at $T > 450$–500°C, the Arai plot is again linear with passing pTRM checks. We interpret this as relatively stable behavior in the homogenous titanomagnetite below the temperature at which cation reordering begins; unstable behavior in the temperature range where (un)blocking and cation reordering take place simultaneously; and stable behavior during unblocking of the low-Ti exsolved phase. Specimens of the first type do not pass any type of quality control criteria and are not interpreted. Specimens of the second two types typically result in paleointensity estimates close to the expected value of 55.7 μT.

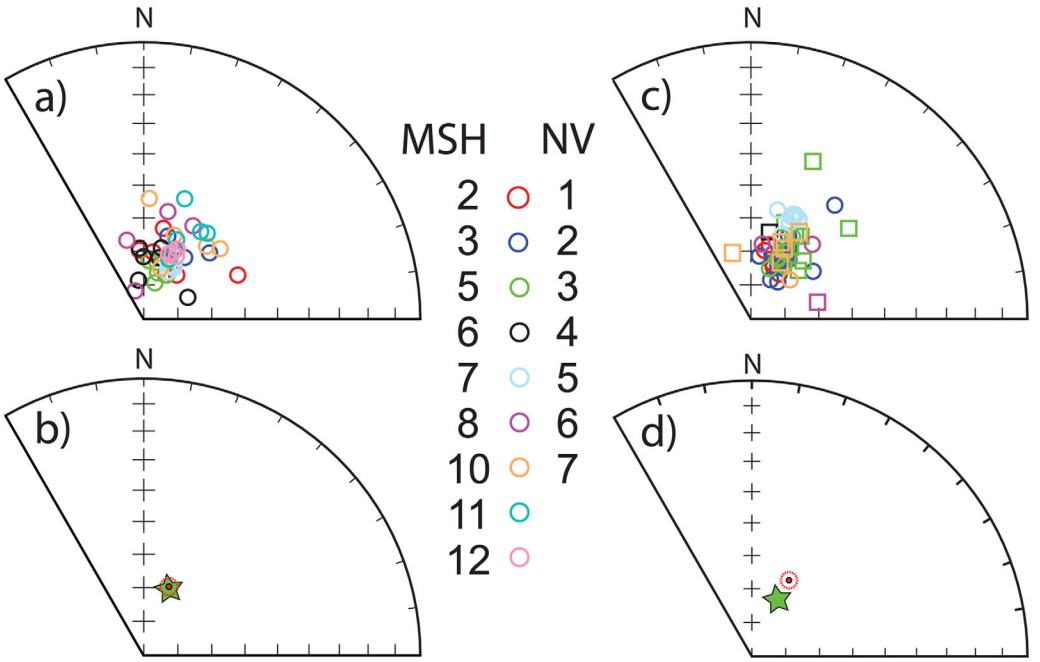

Figure 5. Specimen NRM directions for (a) Mt. St. Helens and (c) Novarupta on equal area plots. All symbols are lower hemisphere. Circles (squares) are thermal (AF) demagnetization. (b, d) Locality means (red dots with dashed α_{95} Fisher confidence ellipses) compared to expected DGRF direction (green star).

4. Discussion

4.1. Magnetic Mineralogy

As noted above, the magnetic mineralogy in samples from both localities is dominated by preeruptive phenocrysts. Reflectance microscopy and thermomagnetic data [*Bowles et al*., 2013; *Jackson and Bowles*, 2014] demonstrate that samples contain variable proportions of two populations of phenocrysts: homogeneous MD titanomagnetite and oxyexsolved titanomagnetite. The presence of a sizable fraction of oxyexsolved grains in most samples reduces the average domain state to PSD, which in this study appears to accurately recover paleointensity in the MSH samples. This is consistent with recent work by *Almeida et al*. [2014] who demonstrate that PSD-sized magnetite effectively behaves in a manner similar to uniaxial SD magnetite up to temperatures very close to T_c.

At MSH, there is some evidence suggesting that the oxyexsolution happened postemplacement, and only in flows with high (>500–600°C) emplacement temperatures [*Jackson and Bowles*, 2014]. The fact that samples dominated by oxyexsolved grains reproduce the known field argues that oxyexsolution occurred at $T > T_c$, or at a high enough temperature that the majority of the remanence is a TRM. Other studies have suggested that oxyexsolution can occur at considerably lower temperatures [e.g., *Smirnov and Tarduno*, 2005, and references therein] but the precise temperature at which oxidation ceases is likely linked to cooling rate and oxygen fugacity.

The same may be true at Novarupta, but many of the samples have clearly undergone low-temperature alteration, which has affected the remanence in a way that is difficult to understand, but likely involves some kind of chemical remanent magnetization (CRM) or thermochemical remanent magnetization (TCRM). The most difficult aspect to explain is the extremely large NRM-pTRM slopes in many specimens at low (<350–400°C) temperatures. While both a TCRM [*Draeger et al*., 2006; *Yamamoto*, 2006; *Fabian*, 2009] and a viscous remanent magnetization (VRM) could result in a higher remanence than a TRM, neither model easily explains an NRM that is up to 5–10 times stronger than the lab-induced pTRM. Results of viscosity experiments confirm that VRM is an unlikely cause for this behavior. (See supporting information text and Figure S4.) Another possible explanation is destruction or transformation of magnetic minerals during heating. However, there is no corresponding loss of room-temperature susceptibility over the same temperature interval that might accompany destruction; rather, susceptibility measured after each heating step either

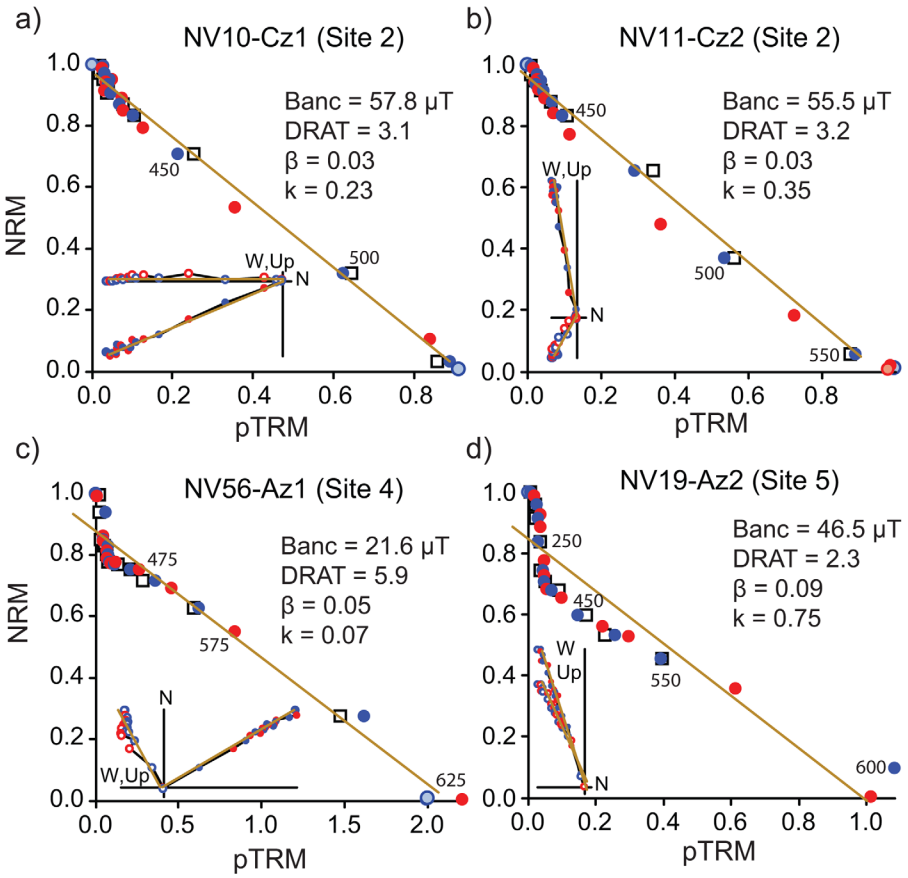

Figure 6. Representative Arai (NRM-pTRM) plots from Novarupta. Best fit lines include all data between 100°C and first point where NRM ≤ 5% starting value. Insets are NRM vector endpoint plots. Blue circles are zero field – in field (ZI) steps. Red circles are in field – zero field (IZ) steps. Lighter shading indicates points not used in slope calculation. Squares are pTRM checks. Banc = paleointensity estimate; DRAT = difference ratio [*Selkin and Tauxe*, 2000]; β = standard error of slope divided by slope [*Coe et al.*, 1978]; k = curvature [*Paterson*, 2011].

increases by up to 15% or decreases by <5%. *Kosterov and Prévot* [1998] observe similar (though not as extreme) behavior in basalts and suggest it is due to domain reorganization, as imaged by *De Groot et al.* [2014].

In addition to the phenocrysts, welding at NV may have also led to some postemplacement growth of glass-hosted magnetite (inferred from density separates), which does not contribute strongly to the remanence. This population is not found in the glassy MSH pumice, perhaps because it cooled too quickly for the magnetite to nucleate and grow.

4.2. Paleointensity Data Processing

Paleointensity results from the two localities are very different, and deviations from ideal behavior appear to be from two different causes. The Novarupta samples have experienced long-lived, low-temperature hydrothermal activity, and this appears to have adversely impacted the magnetization and magnetic mineralogy. Although most specimens are influenced to some degree, if we simply accept all data points in every Arai plot and calculate a paleofield, we see that samples taken from within or directly adjacent to focused hydrothermal fissures deviate more from the expected paleointensity than do samples farther away from these fissures (Figure 4e). By contrast, the MSH paleointensity data can be interpreted in a relatively straightforward manner linked to magnetic mineralogy (section 3.3).

Given the highly nonideal behavior of most of the Novarupta data, we are faced with the reasonable prospect of rejecting it all, or devising a way to calculate paleointensity while appropriately estimating the uncertainty. We have taken two very different approaches, and we suggest that combined they give a full

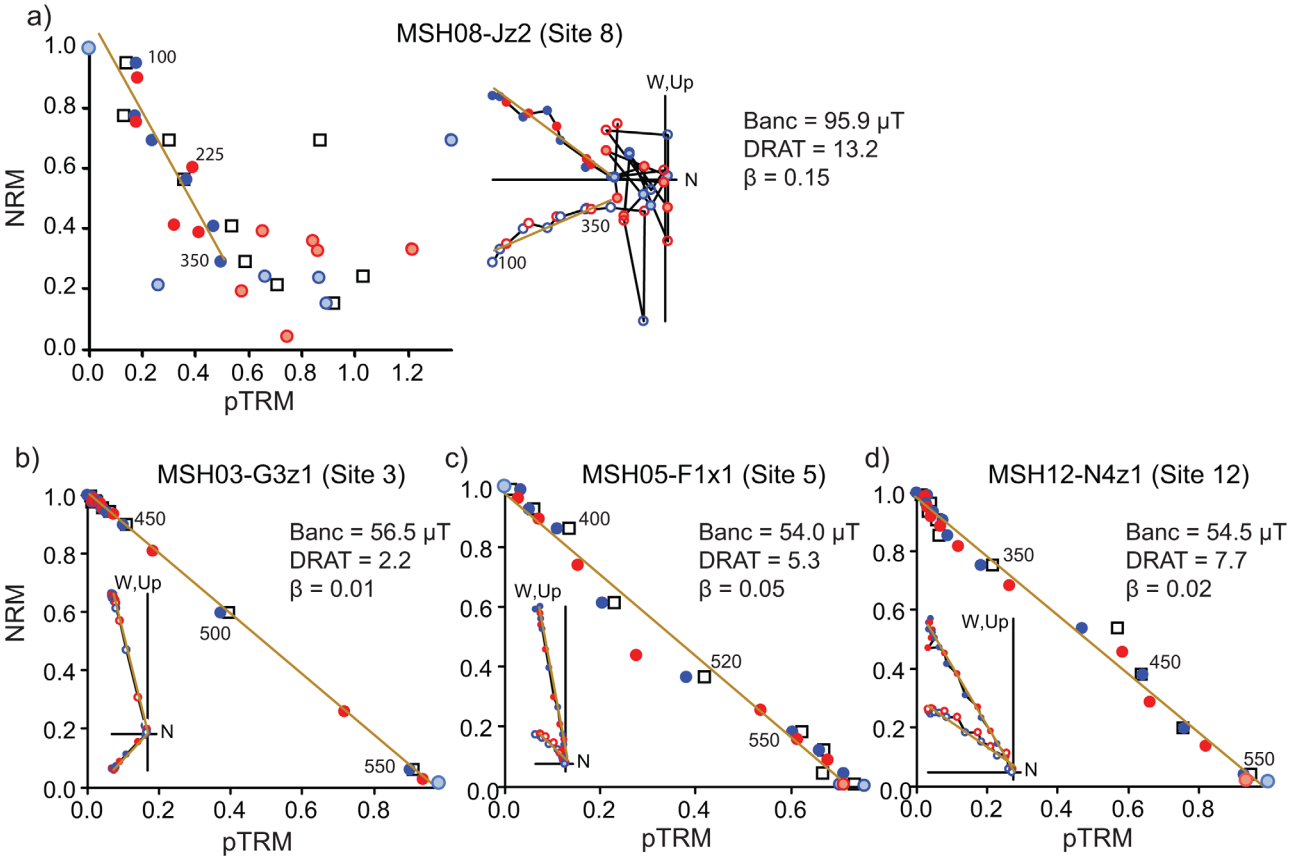

Figure 7. Representative Arai (NRM-pTRM) plots from Mt. St. Helens. Best fit lines as in Figure 6, except for Figure 7a which includes data only up to 350°C to illustration change in behavior at this temperature (see text). If all data were included for this specimen, Banc = 40.8 μT; DRAT = 47.1; β = 0.25. Symbols as in Figure 6.

picture of the uncertainty in the resulting paleointensity. The first approach applies very strict selection criteria to the data, passing only a very small number of well-behaved specimens. The second method takes the opposite approach, applying very lenient selection criteria, but using all the data in a multislope bootstrap approach that incorporates specimen-level uncertainty in the locality mean.

Before we describe these two approaches, we briefly explain the quality-control selection criteria we use. Many parameters have been proposed to test for nonideal behavior in paleointensity experiments (see recent reviews by *Shaar and Tauxe* [2013] and *Paterson et al.* [2014a]).

Here we select parameters that control for (1) nonlinearity in the NRM-pTRM plot and (2) alteration during laboratory heating. To control for nonlinearity, we simply require that the scatter in the best fit slope be low, as estimated by the standard error of the slope divided by the slope [*Coe et al.*, 1978], here denoted β. While *Paterson* [2011] suggests fitting a circle to the Arai plot and taking the curvature (k = 1/radius) as a way to detect nonlinearity in the plot, this parameter was unable to discriminate between a true single-slope plot and a dual-slope plot. The slope shown in Figure 6c is clearly nonlinear, yet it has a low *k* value [*Paterson*, 2011]. Because this test was designed to recognize the curvature or "sag" of MD behavior, it is perhaps not surprising that it does not work here, where the nonlinearity arises from some other cause and an arc will not fit the data well.

To test for alteration during laboratory heating, we require the maximum DRAT to be $\leq$10%. It has been suggested that it is more appropriate to calculate a cumulative DRAT (DRATs or CDRAT), defined as the signed sum of the differences between repeat pTRM steps, normalized by the pTRM acquired by cooling from the maximum temperature step used in the slope calculation to room temperature [*Tauxe and Staudigel*, 2004]. However, using DRATs instead of DRAT in the multislope (bootstrap) approach has the effect of excluding many of the very steep, low-temperature slopes from the NV data set; the resulting DRATs values are very large, because little to no pTRM is gained over this interval.

Finally, in the multislope approach, we do not include slopes that carry a very small fraction of the remanence. We define f^* as the fraction of total NRM held by the slope of interest. In other words, if $T_{min} = 200°C$ and $T_{max} = 400°C$, $f^* = [NRM_{200} - NRM_{400}]/NRM_{tot}$. This is a simpler calculation than most fraction statistics previously used (e.g., f of *Coe et al*. [1978]; f_{vds} of *Tauxe and Staudigel* [2004]; FRAC of *Shaar and Tauxe* [2013]), but it avoids complications arising from noise in the data, and because the NRMs are all unidirectional it does not overestimate the true NRM fraction.

Although it may seem that using a greater number of criteria will produce a more reliable result, we find that typically only a small number of criteria explain the variability in any given data set, depending on the cause(s) of nonideal behavior. Application to this study of any of the suggested selection criteria sets explored in *Paterson et al*. [2014b]—including the PICRIT03 [*Kissel and Laj*, 2004] and SELCRIT2 [*Biggin et al*., 2007] criteria—almost always produces results that deviate more greatly from the known value. (See supporting information Table S4 and Figure S5 for a summary.) For MSH, the deviations are slight for the single-slope case but increase for the bootstrapped case such that the mean no longer overlaps the known value at the 95% confidence level. If f is forced to be ≥ 0.35, the deviations become negligible. For NV, in the single-slope case, failure arises from the relatively lax β threshold (0.1) used by these selection criteria. By contrast, enforcing any β criteria in the bootstrap case results in rejection of all portions of the Arai plot near the break in slope. This final result is a lower average paleointensity.

4.2.1. Single-Slope Approach

The major problem with the NV data lies in the two-slope nature of the Arai plots. To deal with this, we apply an objective selection criterion that only selects single-slope specimens. For each specimen, we calculate β using a single fit to data from all temperature steps between 100°C and the first temperature where the NRM is $\leq 5\%$ of the starting value. To select the cut-off value for β, we calculate the standard deviation of the entire locality mean paleointensity for a range of β between 0.02 and 0.10 (Figure 8a). We find that for both NV and MSH, the dispersion in the data set (as measured by the standard deviation) begins to increase for values of $\beta > 0.04$. We repeat the process with the additional constraint of DRAT ≤ 10, but for low values of β there is little difference in the resulting mean or standard deviation (Figure 8). The resulting locality mean paleointensity estimates (using $\beta \leq 0.04$ as the sole selection criteria) are 56.1 ± 1.14 μT (2 standard error of the mean; 95% confidence bounds) for MSH and 57.4 ± 2.70 μT for NV (Figure 9 and Table 1). Both means are consistent with the expected value at the 95% confidence level. By including the DRAT criterion, the NV mean barely excludes the expected value at this level, but is still within 6% of the expected value. All specimens processed in this way are listed in supporting information Tables S2 and S3.

At the site level, the MSH results show some intersite variability, with site averages ranging from 52.8 to 59.7 μT (no DRAT) or 49.0 to 59.7 μT (DRAT ≤ 10) (supporting information Figure S6). This suggests that it is beneficial to sample both widely and abundantly in order to average out small local variations that may arise from local crustal magnetic anomalies or other sources. Of the 14 passing specimens from NV, all but two are from a single site (site 2), which may partially explain why the NV mean deviates more from the true value than at MSH. The small number of specimens may also explain why the NV locality mean is sensitive to the exclusion of one additional specimen that results from applying the DRAT criterion (Figures 8 and 9). We therefore take a second approach whereby all data from all specimens are included in a bootstrap resampling process.

4.2.2. Multislope (Bootstrap) Approach

When interpreting Arai plots, one approach is to select a single temperature range and calculate one slope over this range (as above). The investigator is guided by experimental evidence of viscous overprints or thermochemical alteration, but ultimately the selection is somewhat subjective. When two slopes are present, a decision must be made to interpret one or the other, and in the absence of pTRM check failures, the high-temperature slope is typically selected.

Here we take a completely different approach that assumes that the "true" answer lies somewhere in the range of the data and explores all possible solutions, rather than subjectively selecting a single solution. We conduct this bootstrap resampling (or "multislope") approach in several ways to test the sensitivity of the results. First, we take the approach of *Bowles et al*. [2005] (denoted JB in Table 1), where all possible slopes of ≥ 4 continuous points are calculated (subject to the constraints described below). The specimen mean is taken to be the mean of these slopes, and the scatter in the data is represented by standard deviation of the mean. To find the locality mean, we conduct a bootstrap resampling (with replacement) of the N specimens, whereby a specimen is chosen at random, and its mean paleointensity is perturbed by a random Gaussian deviate about the standard

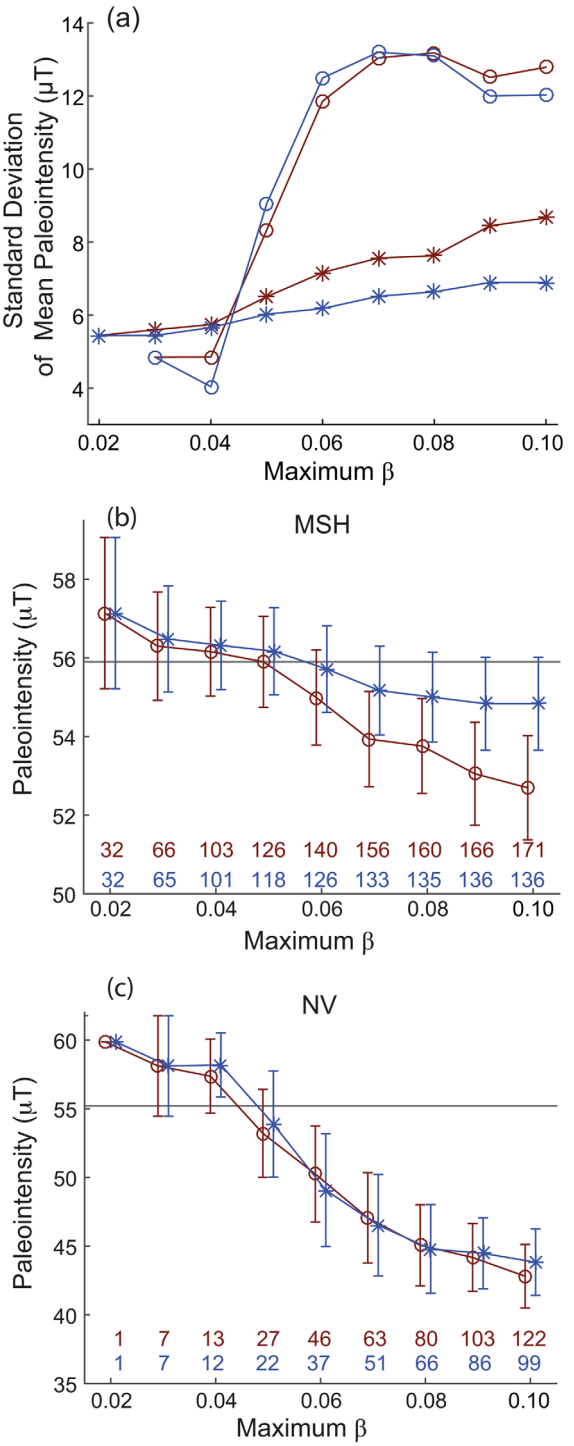

Figure 8. Results of single-slope analysis. (a) Variation in *standard deviation* of paleointensity mean calculated via the single-slope method, as a function of the maximum allowed β. Circles are NV, stars are MSH. Red symbols are calculated using β as the only discriminant. Blue symbols additionally reject any specimens with DRAT $>$ 10. Variation in locality mean paleointensity for (b) MSH and (c) NV. Error bars represent 95% confidence bounds (2 *standard error* of the mean). Red circles are means calculated using β as the only discriminant. Blue stars additionally reject any specimens with DRAT $>$ 10. Numbers at bottom of charts represent the number of specimens included in the mean. Data are shifted slightly so all error bars are visible.

deviation. This is repeated N times, and the mean of the N paleointensity estimates is 1 bootstrapped mean. The entire resampling process is repeated 10,000 times, and the mean of the 10,000 bootstrap means is taken to be the locality mean. We require that each individual slope have an f* value $>$ 0.4. We repeat the process with the additional constraint that individual slope DRAT $\leq$ 10. Results are detailed in Table 1 and Figure 9.

We compare these results to those obtained from a similar approach taken by *Shaar and Tauxe* [2013] which we reproduce here. Instead of calculating a specimen-level paleointensity mean and standard deviation from the acceptable slopes, the *Shaar and Tauxe* [2013] bootstrap resampling process selects one of the permissible specimen slopes at random. They call this the "nonparametric" approach (denoted RSnp in Table 1), and contrast it with a "parametric" approach (RSp), where the true specimen-level paleointensity is assumed to lie within the interval defined by the maximum and minimum permissible slopes. During the bootstrap resampling in the parametric approach, a value is randomly selected within this interval, assuming a uniform distribution function. We apply the same individual slope f* and DRAT constraints.

For the MSH data, which are generally of high technical quality, the approach chosen does not strongly affect the results. The exception is the bootstrap approach without the DRAT constraint that results in a locality mean that is slightly too low, and does not overlap the known value at the 95% confidence level (JB and RSnp Figure 9). The DRAT criterion therefore appears to effectively discriminate against specimens that may be altering or undergoing cation reordering during experimental reheating.

For the NV data, the results are more variable depending on the approach, but with the exception of the parametric bootstrap, all methods overlap the true field at the 95% confidence level (Figure 9). The parametric bootstrap appears to give too much weight to the steep, low-temperature slopes. As with the MSH data, the multislope approach unconstrained by DRAT results in lower paleofield estimates, but in this case the uncertainty is larger and still encompasses the known value.

In the NV case, with one steep and one shallow slope, the assumption that the "true" answer

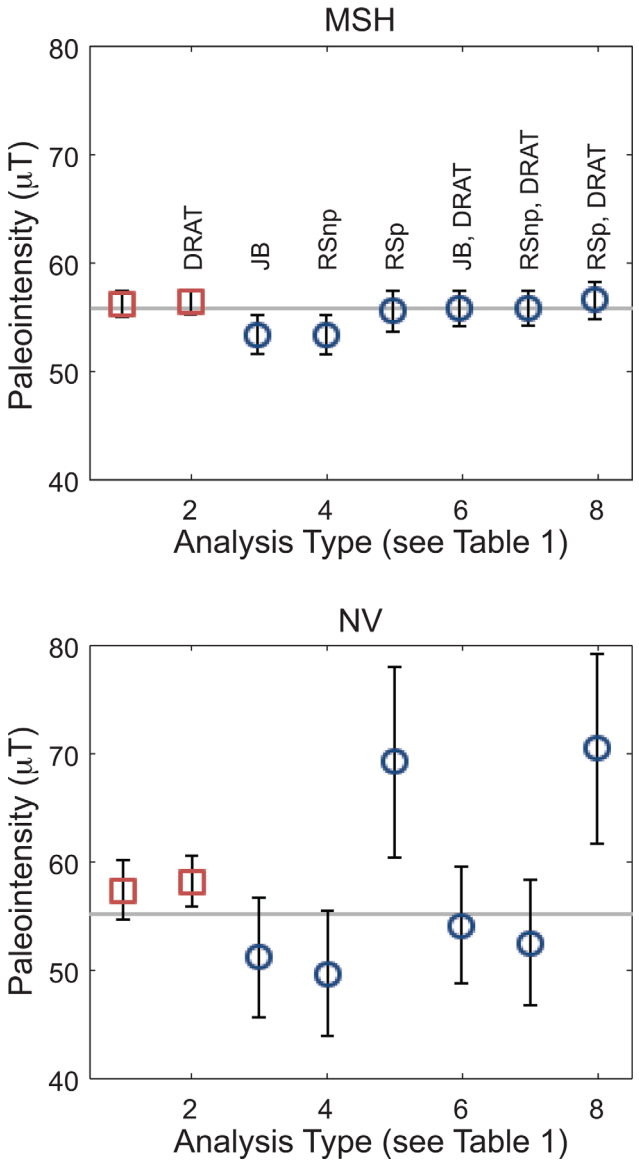

Figure 9. Summary of paleointensity interpretations. Locality means as shown in Table 1. Error bars are 95% confidence intervals. Horizontal gray line is expected DGRF field value. Numbers on horizontal axis keyed to Table 1. Red squares are single-slope analyses. Blue circles are bootstrap analyses. DRAT indicates additional constraint of DRAT $\leq$ 10 imposed. See text and Table 1 for abbreviation explanations.

lies somewhere in the range of the data is likely correct, but the agreement between the bootstrapped result and the true value may be coincidental. The method only reproduces the range of uncertainty represented by the actual data, and in cases where the sample carries a total CRM or TCRM, the true value may not be contained within the available data. Likewise, if samples alter at moderate temperature, failed pTRM checks would exclude all slopes in the high-temperature range, and the low-temperature slope would dominate the result. The technique is perhaps most useful when there is significant noise in the NRM-pTRM data or when two slopes are present and it is unclear which is the correct one. In the present case, the fact that the bootstrapped result agrees with the (few) single-slope results gives added confidence to the overall result.

4.3. Interpretation

We now address the results in the context of emplacement temperature and postemplacement alteration. In the MSH samples, emplacement temperature has an indirect effect on paleointensity by controlling the

Table 1. Summary of Paleointensity Locality Means

	Method[a]	Additional Constraints[b]	Mean (μT)	95% conf. (μT)[c]	N
Mt. St. Helens (55.7 μT)					
1	Single slope	$\beta \leq 0.04$	56.1	1.14	103
2	Single slope	$\beta \leq 0.04$; DRAT ≤ 10	56.3	1.12	101
3	Bootstrap, JB	$f^* \geq 0.4$; $N_{pts} \geq 4$	53.3	1.74	189
4	Bootstrap, RSnp	$f^* \geq 0.4$; $N_{pts} \geq 4$	53.3	1.76	189
5	Bootstrap, RSp	$f^* \geq 0.4$; $N_{pts} \geq 4$	55.5	1.92	189
6	Bootstrap, JB	$f^* \geq 0.4$; $N_{pts} \geq 4$; DRAT ≤ 10	55.7	1.62	164
7	Bootstrap, RSnp	$f^* \geq 0.4$; $N_{pts} \geq 4$; DRAT ≤ 10	55.7	1.58	164
8	Bootstrap, RSp	$f^* \geq 0.4$; $N_{pts} \geq 4$; DRAT ≤ 10	56.4	1.70	164
Novarupta (55.2 μT)					
1	Single slope	$\beta \leq 0.04$	57.4	2.70	13
2	Single slope	$\beta \leq 0.04$; DRAT ≤ 10	58.2	2.34	12
3	Bootstrap, JB	$f^* \geq 0.4$; $N_{pts} \geq 4$	51.2	5.52	139
4	Bootstrap, RSnp	$f^* \geq 0.4$; $N_{pts} \geq 4$	49.7	5.82	142
5	Bootstrap, RSp	$f^* \geq 0.4$; $N_{pts} \geq 4$	69.2	8.78	142
6	Bootstrap, JB	$f^* \geq 0.4$; $N_{pts} \geq 4$; DRAT ≤ 10	54.2	5.42	134
7	Bootstrap, RSnp	$f^* \geq 0.4$; $N_{pts} \geq 4$; DRAT ≤ 10	52.6	5.82	137
8	Bootstrap, RSp	$f^* \geq 0.4$; $N_{pts} \geq 4$; DRAT ≤ 10	70.4	8.76	137

[a]JB denotes approach used in *Bowles et al.* [2005]. RSnp and RSp are the nonparametric and parametric approaches from *Shaar and Tauxe* [2013].

[b]Additional constraints applied to bootstrapped specimens are applied at the individual slope level (see text).

[c]95% confidence bounds for single slope case calculated as two times the standard error (SE) of the mean, where SE is estimated as the estimated standard deviation divided by $\sqrt{N}$. In the bootstrap case, 95% confidence bounds are taken as the interval that contains 95% of the bootstrapped means.

fraction of oxyexsolved grains. Sites for which we have evidence for low emplacement temperature (MSH Sites 2, 8) are dominated by homogeneous, MD titanomagnetite that undergoes cation reordering during laboratory heating. The location of MSH site 8 is at the northernmost edge of the pumice plain, which is dominated by the 18 May flow. Further, it is capped by a characteristic ash layer ~50 cm thick, which we attribute to the air fall from the Plinian column on 18 May. Measured emplacement temperatures for the 18 May flow near our site 8 are ~350°C [*Banks and Hoblitt*, 1996; *Jackson and Bowles*, 2014]. Site 2 is harder to assign to a specific eruption because flow unit boundaries overlap, and it is difficult to distinguish one flow from another in outcrop. However, thermal demagnetization of incorporated lithic fragments show removal of a low-temperature overprint in the direction of the present field at ~275°C, which is interpreted to be the emplacement temperature [e.g., *Hoblitt and Kellogg*, 1979], assuming equivalence of blocking and unblocking temperatures. Paleointensity results from these two sites are largely unsuccessful. By contrast, sites emplaced at higher temperatures have a higher proportion of oxyexsolved grains, which have a smaller effective grain size and are not subject to cation reordering. These sites are largely successful.

At Novarupta, both the short, high-temperature fumarolic activity and the longer, low-temperature vapor phase alteration have clearly had an impact on the magnetization of the NV samples. Samples within and immediately adjacent to visibly leached zones of focused high-temperature fumarolic activity have paleointensities that are significantly lower than both the true value and than other samples (Figure 4e). Samples away from these concentrated zones still mostly show nonideal behavior in the form of two-slope Arai plots, but the deviation from the known field intensity is not as severe.

As hydrothermal alteration (both focused and diffuse) is clearly damaging to paleointensity results, care should be taken to avoid hydrothermally altered areas. The visibly altered, low-susceptibility zones are easy to avoid, yet samples adjacent to these zones but with "normal" magnetic properties and color also have paleointensities that deviate strongly from the true value, especially on either side of the leached zone at ~0.5 m (Figure 4e). As an additional check on postemplacement alteration, we plot deviation from known field value against LOI (Figure 10). Now the samples which had "normal" magnetic properties but highly deviant paleointensities plot in the field with high LOI. There is a clear distinction between specimens with $>0.75\%$ LOI which deviate from the true field value by ~60–80%, and samples with $<0.75\%$ LOI which deviate by less than ~20%. While 20% deviation is not ideal, it may be acceptable depending on the goals of the study. We do not suggest that a 0.75% LOI cutoff is universally applicable, as the water content is likely to reflect both preeruptive water and posteruptive hydration, but large variations in LOI linked to

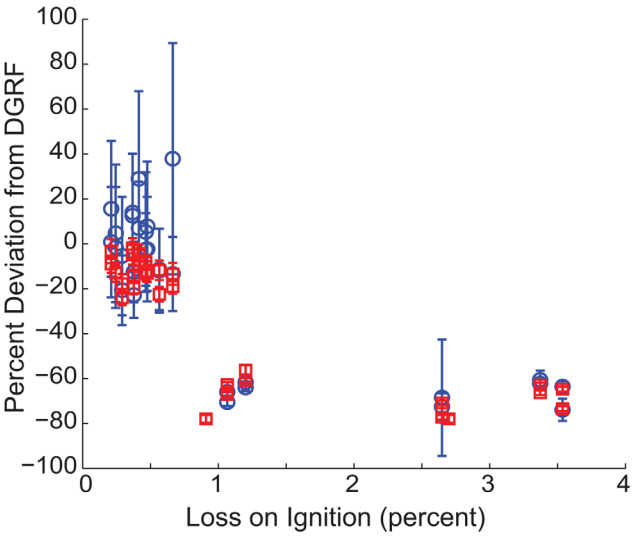

Figure 10. Percent deviation from DGRF paleointensity value (55.2 μT) as a function of loss on ignition (LOI) for Novarupta specimens. Red squares are single-slope analyses. (Note that none would pass the criteria given in the main text). Error bars are derived from standard deviation of the Arai slope. Blue circles are multislope analyses (JB, see main text) with one standard deviation of all permissible slopes. Samples with $<$0.75% LOI have paleointensities clustered between $\pm$20% of DGRF value, while samples with $>$0.75% LOI have paleointensities that deviate by 60% or more from the DGRF value.

variation in paleointensity is a red flag. *Ferk et al.* [2012] find a similar pattern in rhyolitic obsidian, where lower paleointensities are associated with greater hydration. In that case, however, the most hydrated samples had lower coercivity, whereas the most altered samples from NV site 4 have elevated coercivity. Although the mineral assemblage carrying the NRM may be different, the alteration process in both cases appears to result in a CRM that is lower than the corresponding TRM.

Taken as a whole, the data from both localities suggest that PDCs can be suitably used for paleointensity studies, but that just as in any paleointensity study care should be taken to identify potential postemplacement alteration at $T < T_c$. In this respect, larger, welded flows are more likely to undergo focused fumarolic or vapor phase alteration, and should be subjected to extra scrutiny. These larger PDCs may yield reliable paleointensities, but careful documentation of the thermal and alteration history and of the internal consistency of paleofield estimates appear to be advisable.

PDCs that are not dominated by glass-hosted magnetite may still contain abundant PSD magnetite in oxyexsolved phenocrysts, and in this respect they are very similar to basalt flows. One potential advantage over lava flows is the greater areal (or spatial) extent of most PDCs which allows for much more extensive sampling and a better assessment of errors and uncertainty in paleointensity estimates. We strongly recommend always sampling as widely as possible, given the limitations imposed by available outcrop.

In the interpretation of less than ideal data (i.e., specimens lacking a single, linear Arai slope), we suggest that one either completely reject them, or use multiple approaches as a means of better assessing the uncertainty in the resulting paleointensity estimate. In the case of the NV data, the most dangerous thing to do would be to reject the steep, low-temperature slope (as a viscous overprint, e.g.) and analyze just the high-temperature data.

5. Conclusions

Samples from the historical 1912 Novarupta ash flow and the 1980 Mt. St. Helens flows were collected to assess the use of PDCs in paleointensity studies, and to test the effects of emplacement temperature and postemplacement fumarolic or vapor phase alteration on paleointensity estimates. Compared to previous paleointensity work on PDCs, these flows were sampled much more extensively, and by working with historical flows, we can compare results to known field values.

NRM is carried by variable fractions of homogeneous, MD titanomagnetite and oxyexsolved titanomagnetite with an effective PSD grain size. The homogeneous titanomagnetite undergoes cation reordering in the temperature interval of ~350–500°C, leading to unstable remanence behavior.

At MSH, flows emplaced at low (<350°C) temperatures are dominated by homogenous titanomagnetite, leading to an indirect effect of emplacement temperature on paleointensity estimates. Almost all NV specimens have a distinct two-slope behavior in the NRM-pTRM plot that we attribute at least partially to a (T)CRM acquired during postemplacement vapor phase alteration. The largest deviations from the known field value are found in samples with the highest water contents and closest to fossil fumarole zones.

We took two contrasting approaches to interpreting the data. The first applies very stringent selection criteria, accepting only those specimens with a linear NRM-pTRM plot over the entire temperature range. The second approach applies very lenient criteria, but uses all of the data in a multislope bootstrap approach that incorporates specimen-level uncertainty into the locality mean. In cases where the technical quality of the paleointensity data are generally high (as at MSH), the results are insensitive to the approach used. In cases where the technical quality is generally low (as at NV), the variability with approach used more accurately reflects the true uncertainty in these samples with two slope behavior. Although this latter result may not be universally true depending on the nature of the (T)CRM in other samples, we find it advisable to take multiple approaches to interpreting the data.

We find that PDCs can be safely used for paleointensity studies, but that care should be taken in identifying potential postemplacement alteration at $T < T_c$. One advantage in using PDCs over basalt flows lies in the greater areal extent of PDCs, which allows for more extensive sampling and a better assessment of errors and uncertainty.

Acknowledgments

This work was supported by National Science Foundation grants EAR-0944067 and EAR-1315845 (to J.A.B. and M.J.J.) and EAR-0943999 (to J.S.G.) and through support from the NSF Instruments and Facilities program for the Institute for Rock Magnetism. Samples were collected at the Katmai National Park with permission from the National Park Service and under permit number KATM-2010-SCI-0014. Samples were collected at Mt. St. Helens National Monument under permit number MSH-17-2010. We thank Jason Steindorf, John Bowar, and Jesse Vavrek for their help in sample collection, and J. Steindorf and J. Bower for assistance with sample measurements. Constructive comments by Pierre Camps, Greig Paterson, and one anonymous reviewer improved the manuscript. *PmagPy* software provided by Lisa Tauxe was used to process and plot NRM directional data. Samples used in this research are registered with unique identifiers (IGSN) through geosamples.org. All magnetic data presented in this paper are available from the Magnetics Information Consortium (MagIC) database (earthref.org/MAGIC/). This is IRM contribution 1413.

References

Almeida, T. P., T. Kasama, A. R. Muxworthy, W. Williams, L. Nagy, and R. E. Dunin-Borkowski (2014), Observing thermomagnetic stability of nonideal magnetite particles: Good paleomagnetic recorders?, *Geophys. Res. Lett.*, *41*, 7041–7047, doi:10.1002/2014GL061432.

Avery, M. S., J. S. Gee, J. A. Bowles, and M. J. Jackson (2012), Magnetic property variation with vapor-phase alteration in the Bishop Tuff, and implications for paleointensity studies, Abstract GP21A-G1146 presented at 2012 Fall Meeting, AGU, San Francisco, Calif.

Banks, N. G., and R. P. Hoblitt (1996), *Direct Temperature Measurements of Deposits, Mount St. Helens, Washington, 1980-1981*, USGS Prof. Paper 1387, 83 pp., U.S. Gov. Print. Off., Washington, D. C.

Biggin, A. J., M. Perrin, and M. J. Dekkers (2007), A reliable absolute palaeointensity determination obtained from a non-ideal recorder, *Earth Planet. Sci. Lett.*, *257*, 545–563.

Biggin, A. J., G. H. M. A. Strik, and C. G. Langereis (2009), The intensity of the geomagnetic field in the late-Archaean: New measurements and an analysis of the updated IAGA palaeointensity database, *Earth Planets Space*, *61*, 9–22.

Bowles, J., J. Gee, D. V. Kent, E. Bergmanis, and J. M. Sinton (2005), Cooling rate effects on paleointensity estimates in submarine basaltic glass and implications for dating young flows, *Geochem. Geophys. Geosyst.*, *6*, Q07002, doi:10.1029/2004GC000900.

Bowles, J. A., M. J. Jackson, T. S. Berquó, P. A. Sølheid, and J. S. Gee (2013), Inferred time- and temperature-dependent cation ordering in natural titanomagnetites, *Nat. Commun.*, *4*, 1916, doi:10.1038/ncomms2938.

Camps, P., B. S. Singer, C. Carvallo, A. Goguitchaichvili, G. Fanjat, and B. Allen (2011), The Kamikatsura event and the Matuyama–Brunhes reversal recorded in lavas from Tjörnes Peninsula, northern Iceland, *Earth Planet. Sci. Lett.*, *310*, 33–44.

Christiansen, R. L., and Peterson, D. W. (1981), Chronology of the 1980 eruptive activity, in *The 1980 Eruptions of Mount St. Helens, Washington*, USGS Prof. Paper 1250, edited by P. W. Lipman and D. R. Mullineaux, pp. 17–30, U.S. Dep. of the Inter., U.S. Geol. Surv., Washington, D. C.

Coe, R. S. (1967a), The determination of paleo-intensities of the Earth's magnetic field with emphasis on mechanisms which could cause non-ideal behavior in Thellier's method, *J. Geomagn. Geoelectr.*, *19*, 157–179.

Coe, R. S. (1967b), Paleo-intensities of the Earth's magnetic field determined from Tertiary and Quaternary rocks, *J. Geophys. Res.*, 72, 3247–3262.

Coe, R. S., S. Gromme, and E. A. Mankinen (1978), Geomagnetic paleointensities from radiocarbon-dated lava flows on Hawaii and the question of the Pacific nondipole low, *J. Geophys. Res.*, *83*, 1740–1756.

De Groot, L. V., K. Fabian, I. A. Bakelaar, and M. J. Dekkers (2014), Magnetic force microscopy reveals meta-stable magnetic domain states that prevent reliable absolute palaeointensity experiments, *Nat. Commun.*, *5*, 4548, doi:10.1038/ncomms5548.

Draeger, U., M. Prevot, T. Poidras, and J. Riisager (2006), Single-domain chemical, thermochemical and thermal remanences in a basaltic rock, *Geophys. J. Int.*, *166*, 12–32, doi:10.1111/j.1365-246X.2006.02862.x.

Dunlop, D. J. (2002), Theory and application of the Day plot (Mrs/Ms versus Hcr/Hc): 1. Theoretical curves and tests using titanomagnetite data, *J. Geophys. Res.*, *107*(B3), 2056, doi:10.1029/2001JB000486.

Dunlop, D. J., and C. J. Hale (1976), A determination of paleomagnetic field intensity using submarine basalts drilled near the Mid-Atlantic Ridge, *J. Geophys. Res.*, *81*, 4166–4172.

Fabian, K. (2003), Some additional parameters to estimate domain state from isothermal magnetization measurements, *Earth Planet. Sci. Lett.*, *213*, 337–345.

Fabian, K. (2009), Thermochemical remanence acquisition in single-domain particle ensembles: A case for possible overestimation of the geomagnetic paleointensity, *Geochem. Geophys. Geosyst.*, *10*, Q06Z03, doi:10.1029/2009GC002420.

Ferk, A., J. S. Denton, R. Leonhardt, H. Tuffen, S. Koch, K. U. Hess, and D. B. Dingwell (2012), Paleointensity on volcanic glass of varying hydration states, *Phys. Earth. Planet. Inter.*, *208*, 25–37.

Fierstein, J., and C. J. N. Wilson (2005), Assembling and ignimbrite: Compositionally defined eruptive packages in the 1912 Valley of Ten Thousand Smokes ignimbrite, Alaska, *GSA Bull.*, *117*, 1094–1107, doi:10.1130/B25621.1.
Gee, J. S., Y. Yu, and J. Bowles (2010), Paleointensity estimates from ignimbrites: An evaluation of the Bishop Tuff, *Geochem. Geophys. Geosyst.*, *11*, Q03010, doi:10.1029/2009GC002834.
Geissman, J. W., N. G. Newberry, and D. R. Peacor (1983), Discrete single-domain and pseudo-single-domain titanomagnetite particles in silicic glass of an ash-flow tuff, *Can. J. Earth Sci.*, *20*, 334–338.
Goguitchaichvili, A., L. M. Alva-Valdivia, J. Rosas-Elguera, J. Urrutia-Fucugauchi, and J. Sole (2004), Absolute geomagnetic paleointensity after the Cretaceous Normal Superchron and just prior to the Cretaceous-Tertiary transition, *J. Geophys. Res.*, *109*, B01105, doi:10.1029/2003JB002477.
Herrero-Bervera, E., and J.-P. Valet (2009), Testing determinations of absolute paleointensity from the 1955 and 1960 Hawaiian flows, *Earth Planet. Sci. Lett.*, *287*, 420–433.
Hildreth, W. (1983), The compositionally zoned eruption of 1912 in the Valley of Ten Thousand Smokes, Katmai National Park, Alaska, *J. Volcanol. Geotherm. Res.*, *18*, 1–56.
Hildreth, W. (1987), New perspectives on the eruption of 1912 in the Valley of Ten Thousand Smokes, Katmai National Park, Alaska, *Bull. Volcanol.*, *49*, 680–693.
Hildreth, W., and J. Fierstein (2000), Katmai volcanic cluster and the great eruption of 1912, *GSA Bull.*, *112*, 1594–1620.
Hoblitt, R. P., and K. S. Kellogg (1979), Emplacement temperatures of unsorted and unstratified deposits of volcanic rock debris as determined by paleomagnetic techniques, *GSA Bull.*, *90*, 633–642.
Hogeweg, N., T. E. C. Keith, E. M. Colvard, and S. E. Ingebritsen (2005), Ongoing hydrothermal heat loss from the 1912 ash-flow sheet, Valley of Ten Thousand Smokes, Alaska, *J. Volcanol. Geotherm. Res.*, *143*, 279–291.
Holt, E. W., and H. P. Taylor Jr. (2001), 180/160 studies of fossil fissure fumaroles from the Valley of Ten Thousand Smokes, Alaska, *Bull. Volcanol.*, *63*, 151–163.
Jackson, M., and P. Solheid (2010), On the quantitative analysis and evaluation of magnetic hysteresis data, *Geochem. Geophys. Geosyst.*, *11*, Q04Z15, doi:10.1029/2009GC002932.
Jackson, M. J., and J. A. Bowles (2014), Curie temperatures of titanomagnetite in ignimbrites: Effects of emplacement temperatures, cooling rates, exsolution and cation ordering, *Geochem. Geophys. Geosyst.*, *15*, 4343–4368, doi:10.1002/2014GC005527.
Kienle, J. (1991), Depth of the ash flow deposit in the Valley of Ten Thousand Smokes, Katmai National Park, Alaska, *Geophys. Res. Lett.*, *18*, 1533–1536.
Kirschvink, J. L. (1980), The least-squares line and plane and the analysis of palaeomagnetic data, *Geophys. J. R. Astron. Soc.*, *62*, 699–718.
Kissel, C., and C. Laj (2004), Improvements in procedure and paleointensity selection criteria (PICRIT-03) for Thellier and Thellier determinations: Application to Hawaiian basaltic long cores, *Phys. Earth Planet. Inter.*, *147*, 155–169.
Kono, M. (1974), Intensities of the Earth's magnetic field about 60 my ago determined from the Deccan Trap basalts, India, *J. Geophys. Res.*, *79*, 1135–1141.
Kosterov, A. A., and M. Prévot (1998), Possible mechanisms causing failure of Thellier palaeointensity experiments in some basalts, *Geophys. J. Int.*, *134*, 554–572.
Kulakov, E. V., A. V. Smirnov, and J. F. Diehl (2013), Absolute geomagnetic paleointensity as recorded by$\sim$ 1.09 Ga Lake Shore Traps (Keweenaw Peninsula, Michigan), *Stud. Geophys. Geod.*, *57*, 565–584.
Kuntz, M. A., P. D. Rowley, and N. S. MacLeod (1990), Geologic maps of pyroclastic-flow and related deposits of the 1980 eruptions of Mount St. Helens, Washington, *US Geol. Surv., MAP I-1950.*
Lagroix, F., S. K. Banerjee, and M. J. Jackson (2004), Magnetic properties of the Old Crow tephra: Identification of a complex iron titanium oxide mineralogy, *J. Geophys. Res.*, *109*, B01104, doi:10.1029/2003JB002678.
Lanphere, M. A., D. E. Champion, R. L. Christiansen, G. A. Izett, and J. D. Obradovich (2002), Revised ages for tuffs of the Yellowstone Plateau volcanic field: Assignment of the Huckleberry Ridge Tuff to a new geomagnetic polarity event, *GSA Bull.*, *114*, 559–568.
Lowrie, W. (1990), Identification of ferromagnetic minerals in a rock by coercivity and unblocking temperature properties, *Geophys. Res. Lett.*, *17*, 159–162.
Mochizuki, N., T. Maruuchi, Y. Yamamoto, and H. Shibuya (2013), Multi-level consistency tests in paleointensity determinations from the welded tuffs of the Aso pyroclastic-flow deposits, *Phys. Earth Planet. Inter.*, *223*, 40–54, doi:10.1016/j.pepi.2013.05.001.
Özdemir, Ö. (1987), Inversion of titanomaghemites, *Phys. Earth Planet. Inter.*, *46*, 184–196.
Papike, J. J., T. E. C. Keith, M. N. Spilde, K. C. Galbreath, C. K. Shearer, and J. C. Laul (1991), Geochemistry and mineralogy of fumarolic deposits, Valley of Ten Thousand Smokes, Alaska: Bulk chemical and mineralogical evolution of dacite-rich protolith, *Am. Mineral.*, *76*, 1662–1673.
Paterson, G. A. (2011), A simple test for the presence of multidomain behavior during paleointensity experiments, *J. Geophys. Res.*, *116*, B10104, doi:10.1029/2011JB008369.
Paterson, G. A., A. P. Roberts, C. Mac Niocaill, A. R. Muxworthy, L. Gurioli, J. G. Viramonté, C. Navarro, and S. Weider (2010a), Paleomagnetic determination of emplacement temperatures of pyroclastic deposits: An under-utilized tool, *Bull. Volcanol.*, *72*, 309–330.
Paterson, G. A., A. R. Muxworthy, A. P. Roberts, and C. Mac Niocaill (2010b), Assessment of the usefulness of lithic clasts from pyroclastic deposits for paleointensity determination, *J. Geophys. Res.*, *115*, B03104, doi:10.1029/2009JB006475.
Paterson, G. A., L. Tauxe, A. J. Biggin, R. Shaar, and L. C. Jonestrask (2014a), On improving the selection of Thellier-type paleointensity data, *Geochem. Geophys. Geosyst.*, *15*, 1180–1192, doi:10.1002/2013GC005135.
Paterson, G. A., L. Tauxe, A. J. Biggin, R. Shaar, and L. C. Jonestrask (2014b), On improving the selection of Thellier-type paleointensity data, *Geochem. Geophys. Geosyst.*, *15*, 1180–1192, doi:10.1002/2013GC005135.
Perrin, M., L. M. Alva-Valdivia, M. Lopez-Martinez, J. Rosas-Elguera, M. Benammi, J. A. Gonzalez-Rangel, and P. Camps (2013), Palaeomagnetism of the upper volcanic supergroup, southern part of the Sierra Madre Occidental, Mexico, *Geophys. J. Int.*, *193*, 1250–1264.
Prévot, M. (1981), Some aspects of magnetic viscosity in subaerial and submarine volcanic rocks, *Geophys. J. Int.*, *66*, 169–192.
Prévot, M., M. E.-M. Derder, M. McWilliams, and J. Thompson (1990), Intensity of the Earth's magnetic field: Evidence for a Mesozoic dipole low, *Earth Planet. Sci. Lett.*, *97*, 129–139.
Reynolds, R. L. (1977), Paleomagnetism of welded tuffs of the Yellowstone Group, *J. Geophys. Res.*, *82*, 3677–3693.
Rivera, T. A., M. D. Schmitz, J. L. Crowley, and M. Storey (2014), Rapid magma evolution constrained by zircon petrochronology and 40Ar/39Ar sanidine ages for the Huckleberry Ridge Tuff, Yellowstone, USA, *Geology*, *42*, 643–646.
Roperch, P., N. Bonhommet, and S. Levi (1988), Paleointensity of the Earth's magnetic field during the Laschamp excursion and its geomagnetic implications, *Earth Planet. Sci. Lett.*, *88*, 209–219.
Roperch, P., A. Chauvin, J.-L. Le Pennec, and L. E. Lara (2014), Paleomagnetic study of juvenile basaltic–andesite clasts from Andean pyroclastic density current deposits, *Phys. Earth Planet. Inter.*, *227*, 20–29.

Rosenbaum, J. G. (1993), Magnetic grain-size variations through an ash flow sheet: Influence on magnetic properties and implications for cooling history, *J. Geophys. Res.*, *98*, 11,715-11,727.
Rosenbaum, J. G., and R. B. Waitt Jr. (1981), Summary of eyewitness accounts of the May 18 eruption, in *The 1980 Eruptions of Mount St. Helens, Washington*, USGS Prof. Paper 1250, edited by P. W. Lipman and D. R. Mullineaux, pp. 53–68, US Gov. Print. Off., Washington, D. C.
Rowley, P. D., Kuntz, M. A., and MacLeod, N. S. (1981), Pyroclastic-flow deposits, in *The 1980 Eruptions of Mount St. Helens, Washington*, USGS Prof. Paper 1250, edited by P. W. Lipman and D. R. Mullineaux, pp. 489–512, US Govt. Print. Off., Washington, D. C.
Schlinger, C. M., D. Griscom, G. C. Papaefthymiou, and D. R. Veblen (1988a), The nature of magnetic single domains in volcanic glasses of the KBS Tuff, *J. Geophys. Res.*, *93*, 9137–9156.
Schlinger, C. M., J. G. Rosenbaum, and D. R. Veblen (1988b), Fe-oxide microcrystals in welded tuff from southern Nevada: Origin of remanence carriers by precipitation in volcanic glass, *Geology*, *16*, 556–559.
Schlinger, C. M., D. R. Veblen, and J. G. Rosenbaum (1991), Magnetism and magnetic mineralogy of ash flow tuffs from Yucca Mountain, Nevada, *J. Geophys. Res.*, *96*, 6035–6052.
Schnepp, E. (1995), Palaeointensity study of Quaternary East Eifel phonolitic rocks (Germany), *Geophys. J. Int.*, *121*, 627–633.
Selkin, P., and L. Tauxe (2000), Long-term variations in palaeointensity, *Philos. Trans. R. Soc. London A*, *358*, 1065–1088.
Senanayake, W. E., M. W. McElhinny, and P. L. McFadden (1982), Comparison between the Thelliers' and Shaw's palaeointensity methods using basalts less than 5 million years old, *J. Geomagn. Geoelectr.*, *34*, 141–161.
Shaar, R., and L. Tauxe (2013), Thellier GUI: An integrated tool for analyzing paleointensity data from Thellier-type experiments, *Geochem. Geophys. Geosyst.*, *14*, 677–692, doi:10.1002/ggge.20062.
Singer, B. S., B. R. Jicha, D. J. Condon, A. S. Macho, K. A. Hoffman, J. Dierkhising, M. C. Brown, J. M. Feinberg, and T. Kidane (2014), Precise ages of the Réunion event and Huckleberry Ridge excursion: Episodic clustering of geomagnetic instabilities and the dynamics of flow within the outer core, *Earth Planet. Sci. Lett.*, *405*, 25–38.
Smirnov, A. V., and J. A. Tarduno (2005), Thermochemical remanent magnetization in Precambrian rocks: Are we sure the geomagnetic field was weak?, *J. Geophys. Res.*, *110*, B06103, doi:10.1029/2004JB003445.
Takai, A., H. Shibuya, A. Yoshihara, and Y. Hamano (2002), Paleointensity measurements of pyroclastic flow deposits co-born with widespread tephras in Kyushu Island, Japan, *Phys. Earth Planet. Inter.*, *133*, 159–179.
Tanaka, H., A. Otsuka, T. Tachibana, and M. Kono (1994), Paleointensities for 10–22 ka from volcanic rocks in Japan and New Zealand, *Earth Planet. Sci. Lett.*, *122*, 29–42.
Tauxe, L., and H. Staudigel (2004), Strength of the geomagnetic field in the Cretaceous Normal Superchron: New data from submarine basaltic glass of the Troodos Ophiolite, *Geochem. Geophys. Geosyst.*, *5*, Q02H06, doi:10.1029/2003GC000635.
Thellier, E., and O. Thellier (1959), Sur l'intensité du champ magnétique terrestre dans le passé historique et géologique, *Ann. Geophys.*, *15*, 285–378.
Till, J. L., M. J. Jackson, J. G. Rosenbaum, and P. Solheid (2011), Magnetic properties in an ash flow tuff with continuous grain size variation: A natural reference for magnetic particle granulometry, *Geochem. Geophys. Geosyst.*, *12*, Q07Z26, doi:10.1029/2011GC003648.
Yamamoto, Y. (2006), Possible TCRM acquisition of the Kilauea 1960 lava, Hawaii: Failure of the Thellier paleointensity determination inferred from equilibrium temperature of the Fe-Ti oxide, *Earth Planets Space*, *58*, 1033–1044.
Yamamoto, Y., H. Tsunakawa, and H. Shibuya (2003), Palaeointensity study of the Hawaiian 1960 lava: Implications for possible causes of erroneously high intensities, *Geophys. J. Int.*, *153*, 263–276.
Yamamoto, Y., H. Shibuya, H. Tanaka, and H. Hoshizumi (2010), Geomagnetic paleointensity deduced for the last 300kyr from Unzen Volcano, Japan, and the dipolar nature of the Iceland Basin excursion, *Earth Planet. Sci. Lett.*, *293*, 236–249.
Yu, Y., L. Tauxe, and A. S. Genevey (2004), Toward an optimal geomagnetic field intensity determination technique, *Geochem. Geophys. Geosyst.*, *5*, Q02H07, doi:10.1029/2003GC000630.
Zies, E. G. (1924), Hot springs of the Valley of Ten Thousand Smokes, *J. Geol.*, *32*, 303–310.